Probing the effect of orbital deformation on the atomic tunneling-ionization-time distribution by phase-of-the-phase spectroscopy

Miao Yu,[1] Yueming Zhou ⊙,[1,*] Min Li ⊙,[1] and Peixiang Lu[1,2]

[1]*School of Physics and Wuhan National Laboratory for Optoelectronics,*
Huazhong University of Science and Technology, Wuhan 430074, China
[2]*Optics Valley Laboratory, Hubei 430074, China*

We theoretically studied the tunneling ionization time of atomic $p_\pm$ orbitals by introducing a weak linearly polarized second-harmonic field to the attoclock frame. In our scheme, the ionization time is retrieved by analyzing the relative phase dependence of ionization yield, where one can be free from handling the Coulomb interaction on the emitted electron. By solving the time-dependent Schrödinger equation, we verified that at low laser intensity the ionization time delays are both close to zero for the $2p_\pm$ orbitals, though their offset angles in the photoelectron angular distributions are different. As the laser intensity increases, the atomic orbitals are deformed significantly, which affects the tunneling-ionization-time distribution. With our scheme, the orbital deformation-induced ionization time delay is unambiguously determined. Furthermore, the depletion of the ground state at the high laser intensity enhances the relative contribution of early ionization events and thus the ionization peak shifts to the earlier time. This effect is also directly revealed by our scheme.

I. INTRODUCTION

Laser-induced electron tunneling is a fundamental nonlinear process in quantum mechanics. A detailed understanding of this dynamics process is particularly necessary, because it is the first step of many interesting phenomena, such as laser-induced diffraction [1–3] and photoelectron holography [4–8]. However, due to the absence of a classical counterpart of the tunneling ionization, the tunneling problem is still controversial, though many experiments and theoretical calculations have been done. Among them, attoclock is currently one of the most useful techniques in obtaining information about the electron tunneling geometry [9,10]. It utilizes an elliptically polarized pulse to map the ionization time of a photoelectron (i.e., the moment at which the photoelectron leaves the tunneling barrier) to its emission angle in the laser polarization plane. The most probable ionization time is extracted from the offset angle of the maximum of the photoelectron momentum distribution (PEMD) with respect to the minor axis of the elliptically polarized laser field. However, the accurate reconstruction of the ionization time from the offset angle presents a formidable theoretical task, which includes the treatment of the Coulomb interaction between the emitted electron and the parent ion, the effect of multielectron correlation, etc. [11]. Several approaches have been proposed to solve these problems, but different conclusions have been drawn. Some experiments and theories declare that tunneling is instantaneous [10,12–24] while others reveal nonzero tunneling time delay [25–31].

Typically, an attoclock uses noble-gas atoms as the experimental targets due to their simple and stable structure. Most of those experimental results were interpreted based on the assumption of a valence s orbital. However, except for helium atoms, the noble-gas atoms naturally carry valence $p_\pm$ orbitals, which has a non-negligible effect on the tunneling-ionization process. It has been shown that the tunneling ionization initiated by strong elliptically polarized laser fields is sensitive to the sense of electron rotation [32–40]. When the rotation direction of the electron is opposite to that of the laser vector field, the ionization rate is significantly higher than the corotating case [32,33]. Moreover, the initial momentum at the tunneling exit of an electron originating from the valence $p_\pm$ orbitals is different, which leads to noticeable differences on the final momentum and attoclock offset angle [36–38]. Recently, it has been shown that the initial valence $p_\pm$ orbitals are deformed and polarized in an elliptically polarized laser field [35,41]. The shape of the electron orbital will significantly affect the tunneling-ionization-time distribution [42]. Therefore, it is necessary to probe the effect of laser-induced orbital deformation on the tunneling-ionization-time distribution in the attoclock frame.

In this work, we resolved the ionization time of photoelectron tunneling from the initial valence $2p_\pm$ orbitals of a model atom by introducing the phase-of-the-phase spectroscopy [43–46] to the attoclock frame. In our scheme, a perturbative second-harmonic field is added to the fundamental driving field. By analyzing the relative phase dependence of the signal in the PEMDs, the ionization time delays of photoelectrons, i.e., the time delay between the maximum electric field of the fundamental laser pulse and the ionization time for the most probable emission angle, are determined. Because our method is free from modeling the Coulomb interaction on the emitted

---

*zhouymhust@hust.edu.cn

electron, the previous debates on identifying the Coulomb-induced deflection angle are avoided. This advantage enables us to explore the effect of laser-dressed atomic orbitals on the tunneling-ionization time. Our results show that at the low laser intensity where the orbital deformation is negligible, the ionization time delays are both close to zero (the instant of maximum electric field) for the $2p_\pm$ orbitals, though the offset angles in the photoelectron angular distributions (PADs) are different. With the increase of laser intensity, the fundamental field induces the deformation of atomic $2p_\pm$ orbitals, which affects the tunneling-ionization-time distributions. Using our scheme, we show that in our model atom, the bound electron initially corotating with the electric field is released at an earlier time compared to that for the counter-rotating case. Furthermore, our results confirm that at high laser intensity the depletion of the ground state significantly modifies the offset angles of the photoelectron angular distributions and the ionization time delays. These depletion-induced negative ionization time delays are also accurately revealed with our method.

The rest of the paper is organized into the following sections. In Sec. II, we introduce the measuring method and numerical model. Our numerical results are presented and analyzed in Sec. III. Finally, we conclude in Sec. IV. Atomic units (a.u.) are used throughout unless otherwise specified.

II. THEORETICAL METHODS

A. Measuring method

Figure 1 illustrates the scheme of our methods. A short circularly polarized 800-nm laser triggers tunneling ionization, the corresponding PEMD is shown in Fig. 1(a). We introduce a weak linearly polarized second-harmonic (SH) field to perturb the fundamental field. The synthesized electric field is written as

$$\mathbf{E}(t,\phi) = E_1 f(t)\{[\cos(\omega t) + \xi\cos(2\omega t + \phi)]\mathbf{e}_x \\ + \sin(\omega t)\mathbf{e}_y\}, \quad (1)$$

with $f(t) = \sin^2[\pi t/(2T)]$ for $0 \leqslant t \leqslant 2T$ and $f(t) = 0$ otherwise. Here, $\mathbf{e}_x$ and $\mathbf{e}_y$ are the unit vectors, and E_1 and $T = 2\pi/\omega$ are the amplitude and optical period of the 800-nm fundamental field, respectively. $\xi = E_{2\omega}/E_\omega$ is the ratio of the electric amplitudes, and ϕ is the relative phase. At a given time t, the synthesized electric field strength is

$$|E(t,\phi)| = \sqrt{E_x^2 + E_y^2} \\ = E_1 f(t)[1 + \xi\cos(\omega t)\cos(2\omega t + \phi)] + O(\xi^2). \quad (2)$$

Due to the perturbative nature of the SH field, we can neglect the small higher-order terms in Eq. (2). Thus, at each given time t, the synthesized electric field strength oscillates with the relative phase of the two-color field and maximizes at the relative phase of

$$\phi_E(t) = -2\omega t. \quad (3)$$

Because the ionization rate exponentially depends on the electric field strength, the photoelectron yield will change
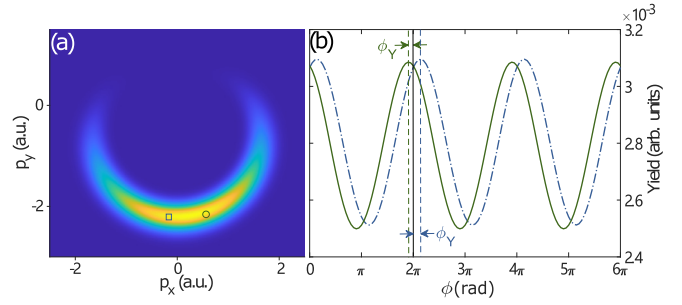
FIG. 1. (a) The PEMD from tunneling ionization initiated by the short circularly polarized laser pulse. (b) For a given momentum, the photoelectron yield oscillates with the relative phase, where the blue dot-dashed line and green solid line correspond to the momenta indicated by the blue box and the green circle in (a), respectively. The optimal phase ϕ_Y indicates the phase maximizing the ionization yield for a given momentum.

significantly with the relative phase, as shown in Fig. 1(b). For different momentum, the optimal phase ϕ_Y where the electron yield maximizes is different. Specifically, if the oscillation of the photoelectron yield for a continuum state $\mathbf{p}$ is in phase with the oscillation of the electric field strength at the instant of t, i.e., $\phi_Y(\mathbf{p}) = \phi_E(t)$, this means that the electron of the continuum state $\mathbf{p}$ is released at the instant of t. Therefore, the tunneling-ionization time for a continuum state $\mathbf{p}$ can be determined by

$$t(\mathbf{p}) = -\phi_Y(\mathbf{p})/(2\omega). \quad (4)$$

In our calculations shown below, the intensity of the SH is 1/6400 of the fundamental field ($\xi = 1/80$). It is sufficiently weak so that the SH-induced change of the final momentum is negligible. This is essential for our scheme.

B. Numerically solving TDSE

To investigate the ionization of a model atom in the two-color field, we numerically solve the two-dimensional time-dependent Schrödinger equation (TDSE) within the single-active-electron approximation. In the length gauge, the TDSE reads

$$i\frac{\partial\Psi_\pm(\mathbf{r},t)}{\partial t} = \left[-\frac{1}{2}\nabla^2 + V(\mathbf{r}) + \mathbf{r}\cdot\mathbf{E}(t,\phi)\right]\Psi_\pm(\mathbf{r},t), \quad (5)$$

where $\Psi_\pm(\mathbf{r},t)$ are the time-dependent wave functions with the $2p_\pm$ orbitals as initial state. $V(\mathbf{r})$ is the effective potential of the model neon atom, which is expressed as [35]

$$V(\mathbf{r}) = -\frac{1 + 9e^{-r^2}}{\sqrt{r^2 + a}}. \quad (6)$$

Here $a = 2.943$ is used to match the ionization potential of neon ($I_p = -E_{2p} = 0.793$ a.u.) for the $2p$ orbital. $\mathbf{r} = (x, y)$ denotes the electron position. Note that the model does not correctly reproduce the energy of the $2s$ orbital [35]. In this model potential, the energy of $2s$ is $E_{2s} = -0.217$ a.u., higher than the $2p$ state, while in the real neon atom $E_{2s} < E_{2p}$. This energy order affects the alignment direction of the deformed orbital [35] and thus the absolute value of the ionization time delay depends on potential we used. In our work, we aim at
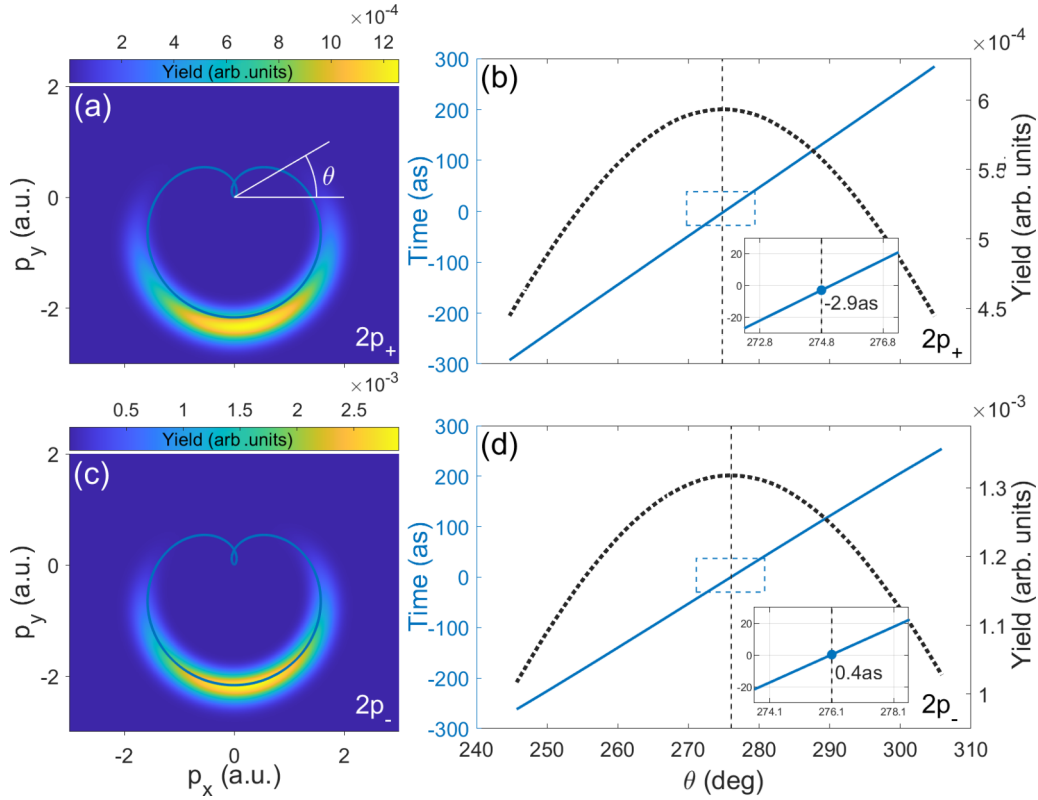
FIG. 2. Ionization dynamics of the model atom starting from the valence $2p_+$ (a), (b) and $2p_-$ (c), (d) orbitals. (a), (c) The calculated PEMDs initiated by the fundamental field with the intensity of 3.0×10^{14} W/cm^2. The blue solid lines indicate the vector potential of the fundamental field. The electron emission angle θ is defined between the electron emission direction relative to the x axis. (b), (d) The retrieved tunneling-ionization time (blue solid line) with respect to the electron emission angle. The black dotted lines and dashed lines represent the radially integrated PADs and corresponding peaks, respectively. The insets show a scale-up of the region inside the blue dashed frames.

revealing the effect of the orbital deformation on the ionization time delay and this model potential is enough to demonstrate this effect.

We use the split-operator method on a Cartesian grid to numerically solve the two-dimensional TDSE [47]. The initial wave function for the $2p_\pm$ orbitals is given by $\Psi^0_\pm = [\Psi_x(\mathbf{r}) + i\Psi_y(\mathbf{r})]/\sqrt{2}$, where the orthogonal normalized eigenfunctions $\Psi_x(\mathbf{r})$ and $\Psi_y(\mathbf{r})$ are prepared by propagating the TDSE in imaginary time and additional orthogonalization procedures at each step [48]. The obtained initial wave function is propagated with Eq. (5). During the propagation, the wave function is split into the inner and the outer parts at time τ (we perform such splitting 30 times per laser cycle),

$$\Psi_\pm(\tau) = \underbrace{\Psi_\pm(\tau)[1 - F_s(R_s)]}_{\Psi^I_\pm(\tau)} + \underbrace{\Psi_\pm(\tau)F_s(R_s)}_{\Psi^o_\pm(\tau)}. \quad (7)$$

Here $F_s(R_s) = 1/[1 + e^{-(r-R_s)/\Delta}]$ is the splitting function that smoothly separates the propagation space into the inner ($0 - R_s$) and outer ($R_s - R_{\max}$) regions, wherein Δ represents the width of the crossover region and R_s is the boundary of the inner space [49]. The inner part wave function $\Psi^I_\pm(\tau)$ is propagated with Eq. (5) and the outer part wave function $\Psi^o_\pm(\tau)$ stands for the "ionization part" and it is propagated under the Volkov Hamiltonian [50,51]. At each time step, the wave function $\Psi^o_\pm(\tau)$ in the outer space is firstly transformed into

the momentum space using

$$C_\pm(\mathbf{p}, \tau) = \int \Psi^o_\pm(\tau) \frac{e^{-i[\mathbf{p}+\mathbf{A}(\tau,\phi)]\cdot\mathbf{r}}}{2\pi} dx\, dy, \quad (8)$$

where $\mathbf{A}(\tau, \phi) = -\int_0^\tau \mathbf{E}(t, \phi)dt$ is the vector potential of the two-color pulse. Then, it is propagated from the time τ to the end of the laser pulse using

$$\bar{C}_\pm(\mathbf{p}, \tau) = e^{-i\int_\tau^{+\infty} 1/2[\mathbf{p}+\mathbf{A}(t)]^2 dt} C_\pm(\mathbf{p}, \tau). \quad (9)$$

Finally, we obtain the PEMD by the relation

$$\frac{dP_\pm(\mathbf{p})}{dE\, d\theta} = \left| \sum_\tau \bar{C}_\pm(\mathbf{p}, \tau) \right|^2, \quad (10)$$

where $E = |\mathbf{p}|^2/2$ is the electron energy and θ is the angle of the emitted electron. In our simulation, the time step of propagation is $dt = 0.04$ a.u. The Cartesian grid ranges from -400 a.u. to 400 a.u. for each direction with a grid size $\Delta x = \Delta y = 0.2$ a.u. The boundary of the inner space is $R_s = 120$ a.u. with $\Delta = 10$ a.u. At the end of the pulse, the wave function is further propagated for an additional two optical cycles to make sure the "slow" electrons reach the boundary R_s [52,53].
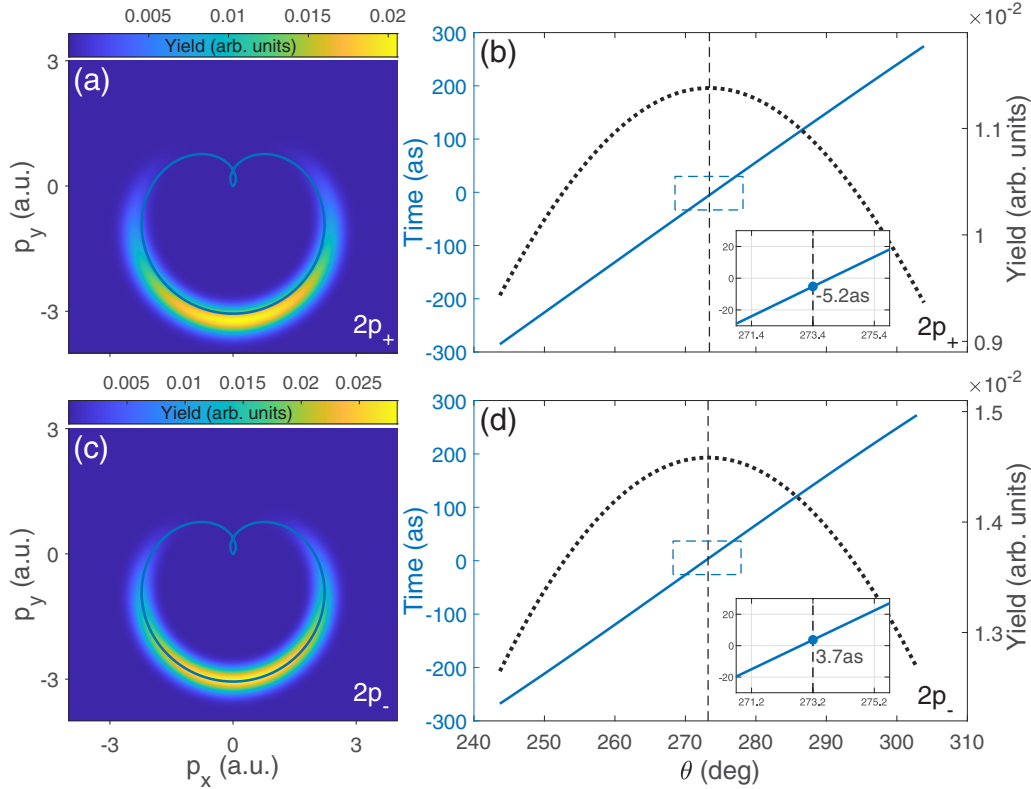
FIG. 3. Same as Fig. 2, but for the stronger fundamental field with the intensity of 6.0×10^{14} W/cm^2, to bring out the laser-dressed $2p_{\pm}$ orbitals.

III. RESULTS AND DISCUSSION

Figures 2(a) and 2(c) show the PEMDs initiated by the fundamental field for tunneling ionization from the valence $2p_+$ and $2p_-$ orbitals, respectively. Here, the laser intensity of the fundamental field is 3.0×10^{14} W/cm^2, and the corresponding time-dependent laser vector potential $-\mathbf{A}(t)$ is displayed as a reference for comparison. In our field configuration, electrons in the $2p_+$ state are corotating and those in the $2p_-$ state are counter-rotating with respect to the right circularly polarized fundamental field. It is shown that the final momentum of the photoelectron from the $2p_+$ orbital is larger than that from the $2p_-$ orbital, in agreement with the previous studies [32,36]. More importantly, there is an angle difference between the peaks of photoelectron distributions corresponding to the ionization from the $2p_{\pm}$ orbitals. This is more clearly in the radially integrated PADs, as shown by the black dotted lines in Figs. 2(b) and 2(d). The offset angles for the valence $2p_+$ and $2p_-$ orbitals are 274.8° and 276.1°, respectively.

To investigate the origin of this angle difference, we retrieve the tunneling-ionization time of photoelectrons ionized from the $2p_{\pm}$ orbitals, which is achieved by using the scheme shown in Fig. 1. Firstly, we add a perturbative SH to the fundamental field. By scanning the relative phase between the two-color laser pulses, we obtain a series of PEMDs. Then we radially integrate over the radial momentum to obtain the PADs. The optimal phase ϕ_Y for different emission angles is further measured by studying the radially integrated photoelectron yield as a function of the relative phase. Finally,

with the optimal phase, the ionization times are determined utilizing Eq. (4). The corresponding results for the $2p_+$ and $2p_-$ orbitals are indicated by the blue solid lines in Figs. 2(b) and 2(d), respectively. By comparing the PAD with the extracted angular-dependent tunneling-ionization time, we find that the position of the most probable emission angles almost coincides with the angle of time zero for the $2p_{\pm}$ orbitals [see the insets in Figs. 2(b) and 2(d)]. These results indicate that the attoclock offset angles of the $2p_{\pm}$ orbitals are entirely from the Coulomb effect of the ionic core, i.e., the ionization time delay is zero, which agrees with the previous theoretical calculation [24].

Strong-field tunneling ionization sensitively depends on the electron orbital of atoms and molecules [42]. In the attoclock experiment, the strong near-circularly polarized laser deforms the atomic $2p_{\pm}$ orbitals, which influences the tunneling ionization and the final momentum distributions. However, determination of this orbital deformation-induced ionization time delay is difficult in the previous attoclock experiments because it requires accurate theoretical calculation of the long-range Coulomb interaction-induced offset angle in the PADs. With our scheme, this difficulty is avoided and the effect of the orbital deformation on the tunneling time distribution could be determined. To demonstrate our scheme, we performed TDSE calculations with a higher laser intensity (6.0×10^{14} W/cm^2) so that the $2p_{\pm}$ orbitals are significantly deformed. The calculated PEMDs (without SH field) for the $2p_+$ and $2p_-$ orbitals are shown in Figs. 3(a) and 3(c), respectively. Compared to the results in Fig. 2, the difference in the ionization yields of the $2p_{\pm}$ orbitals decreases. This is
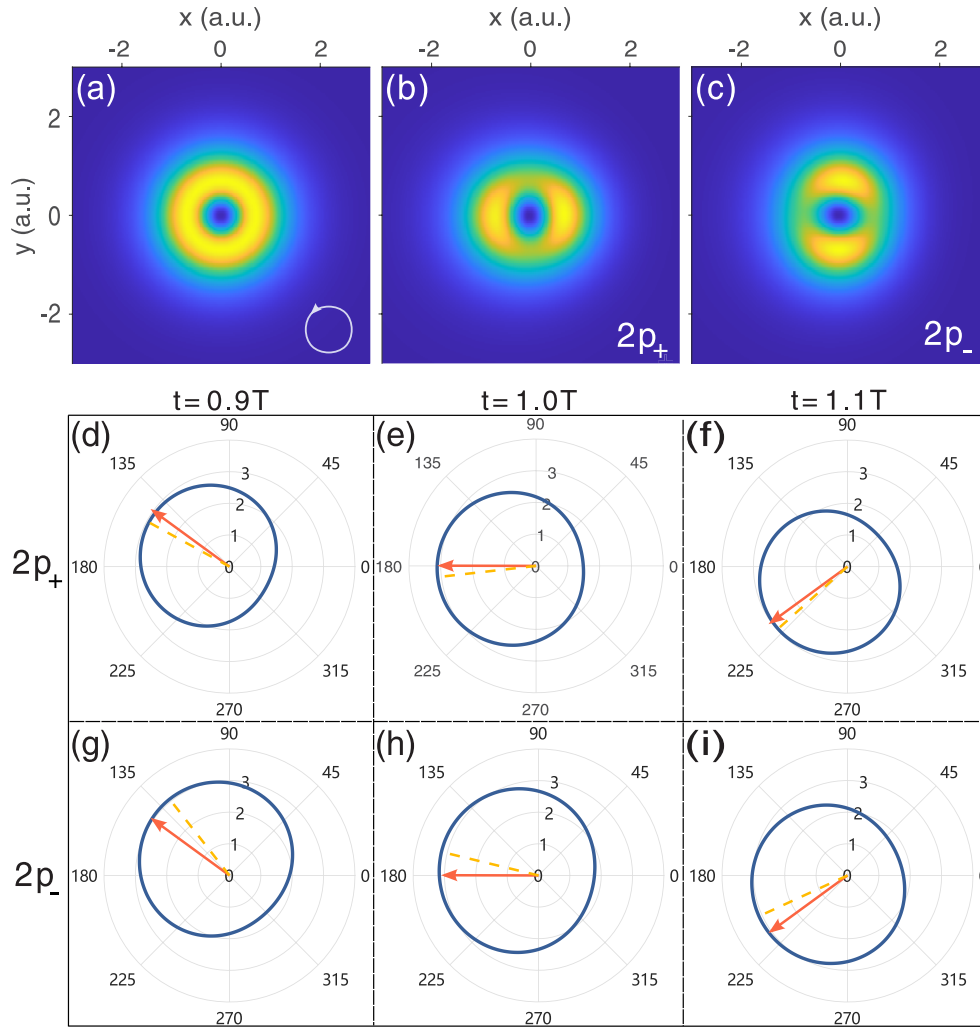
FIG. 4. (a) The initial $2p_\pm$ orbitals of the model atom. The circle with an arrow represent the rotation direction of the laser field. (b), (c) Snapshots of the electron probability densities at time $t_{\max} = T$ for the laser-dressed $2p_+$ (b) and $2p_-$ (c) orbitals. (d)–(i) The electron probability densities (blue curves) along the circle located at $r(t) = I_p/|\mathbf{E}(t)|$ for three instants $0.9T$, $1.0T$, and $1.1T$. The densities are scaled by the factor 10^5 to better display the results. The arrows and dashed lines present the negative instantaneous field vector $(-\mathbf{E})$ and the maximum of the electron probability density, respectively.

one of the phenomena induced by the laser-dressed atomic orbital [35]. Moreover, at this laser intensity, the attoclock offset angles for the $2p_+$ and $2p_-$ orbitals are accidentally identical, being $273.4°$ and $273.2°$, respectively. Using the same method, we retrieve the tunneling-ionization time of different angles, as shown by the blue solid lines in Figs. 3(b) and 3(d). For the $2p_+$ orbital, the ionization time for the photoelectron at the most probable emission angle is shifted to an earlier time of -5.2 as with respect to the instant of the maximum electric field, while for the $2p_-$ orbital it is 3.7 as.

The result indicates that the tunneling-ionization time of a photoelectron is sensitive to the initial direction of rotation of the bound electron at high laser intensity. This phenomenon is caused by the orbital deformation. Figures 4(b) and 4(c) show the instantaneous bound electron probability density $|\Psi_\pm(\mathbf{r}, t_{\max})|$ at the maximum field $t_{\max} = T$ for the $2p_+$ and $2p_-$ orbitals during numerically solving the TDSE. For comparison, the initial $2p_\pm$ orbitals are shown in Fig. 4(a). It displays that the initial $2p_+$ orbital is deformed to the $p_\parallel$

orbital, whose alignment direction is almost parallel to the instantaneous electron field vector. In contrast, the initial $2p_-$ orbital is deformed to the $p_\perp$ orbital that is aligned nearly perpendicular to the instantaneous electric field vector. The formation of two orthogonal states ($p_\parallel$ and $p_\perp$) has been discovered in Ref. [35], where the connections between the bound and deformation states were established analytically by the three-level model. These laser-induced electron density distributions change the relevant instantaneous ionization rate and thus the ionization time distributions are significantly modified. This is more intuitively seen by tracing the electron probability density $|\Psi_\pm(r, t)|$ at the circle located at the position of $r(t) = I_p/|\mathbf{E}(t)|$. Figures 4(d)–4(i) display the electron probability density along this circle at three different instants $t = 0.9T$, $t = 1.0T$, and $t = 1.1T$. Here, the distance between the point on the blue curve and the origin of coordinates represents the magnitude of instantaneous electron probability density. For the $2p_+$ orbital, at the instant of the field maximum, the electron density is not maximized at the
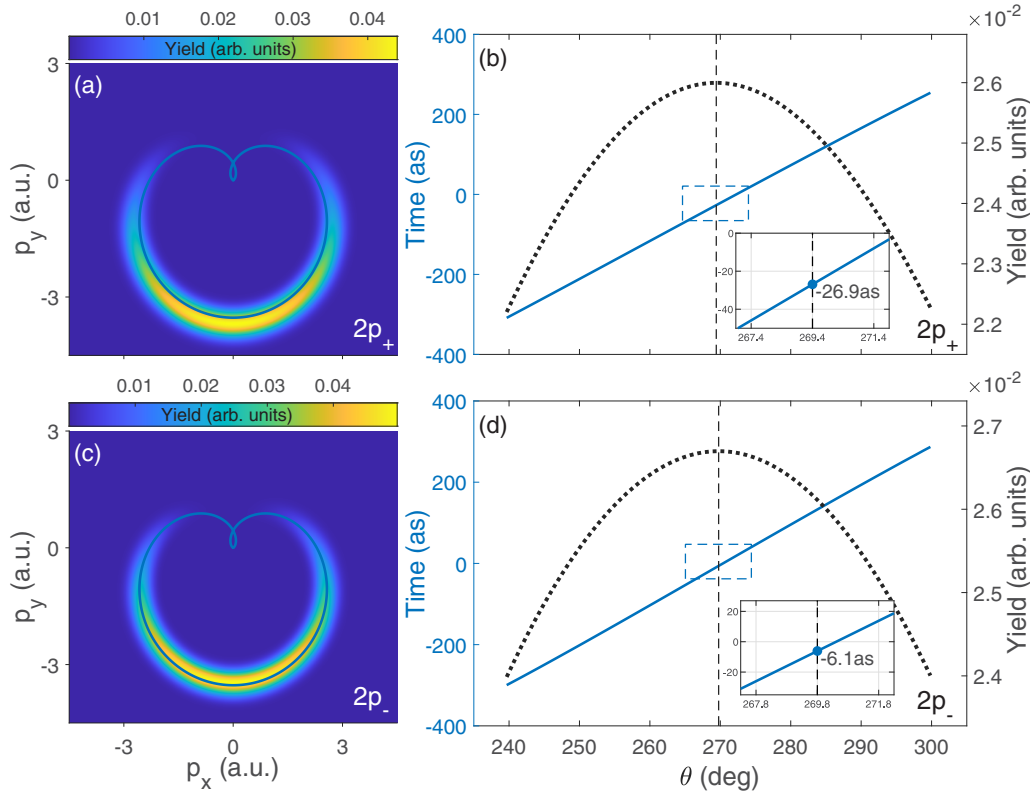
FIG. 5. Same as Fig. 3, but for the stronger fundamental field with the intensity of 8.0×10^{14} W/cm^2.

instantaneous electric field direction. The combined effect of the electric field and electron density distribution leads to the ionization rate maximized before the field maximum, resulting in the negative ionization time delay in our measurement [41]. Similarly, for the $2p_-$ orbital, there should be a positive ionization time delay, as was measured by our method in Fig. 3. These results indicate that the orbital deformation-induced ionization time delays are successfully determined by our method. We mention that in a previous work, the orbital deformation-induced ionization time delay has been traced using the TDSE-based backpropagation method [41]. Here, we provided an experimentally performable method to reveal this effect.

The results above indicate the ionization time delay depends on the laser intensity. To reveal this phenomenon further, we solve the TDSE at a higher laser intensity of the fundamental field, 8.0×10^{14} W/cm^2. The PEMDs initiated by the fundamental field alone for the $2p_+$ and $2p_-$ orbitals are shown in Figs. 5(a) and 5(c), respectively. Figures 5(b) and 5(d) show the radially integrated PADs for the $2p_\pm$ orbitals, where the most probable emission angles locate at 269.4° and 269.8°, respectively. With the same scheme, we determined the tunneling-ionization time for the $2p_\pm$ orbitals, as illustrated in Figs. 5(b) and 5(d). It is shown that the photoelectrons at the most probable emission angle are ionized before the instant of maximum electric field for both the $2p_+$ and $2p_-$ orbitals. For the $2p_+$ orbital, the most probable ionization time is -26.9 as, while for the $2p_-$ orbital it is -6.1 as.

The corresponding instantaneous electron probability density $|\Psi_\pm(r, t)|$ at the circle located at $r(t) = I_p/|\mathbf{E}(t)|$ for three different instants is illustrated in Figs. 6(a)–6(f). It is shown that the orbital deformation becomes more significant at higher laser intensity. Therefore, the difference of the most probable ionization time between the $2p_\pm$ orbitals increases with the laser intensity. In Fig. 6(g), we show the survival probabilities of the wave function as a function of time for the $2p_\pm$ orbitals. It is shown that populations are obviously depleted during the tunneling-ionization process. The loss of population before the maximum field enhances the relative contribution of early ionization events and decreases the attoclock offset angle [13]. Noting that the probability curves in Fig. 6(g) were obtained by projecting the wave function to the field-free ground state and a few excited states. It only provides the information about the survive probability of the bound state approximately, and thus the small time delay difference for the $2p_\pm$ orbitals (about 20 as) could not be revealed by the probability curves. Therefore, as a joint result of orbital deformation and the depletion of the ground state, the most probable ionization times for the $2p_\pm$ orbitals are negative at high laser intensity. This is directly probed by our scheme.

IV. CONCLUSION

We have determined the tunneling-ionization time of a photoelectron from the $2p_\pm$ orbitals over a wide range of laser intensity. This is achieved by introducing the phase-of-the-
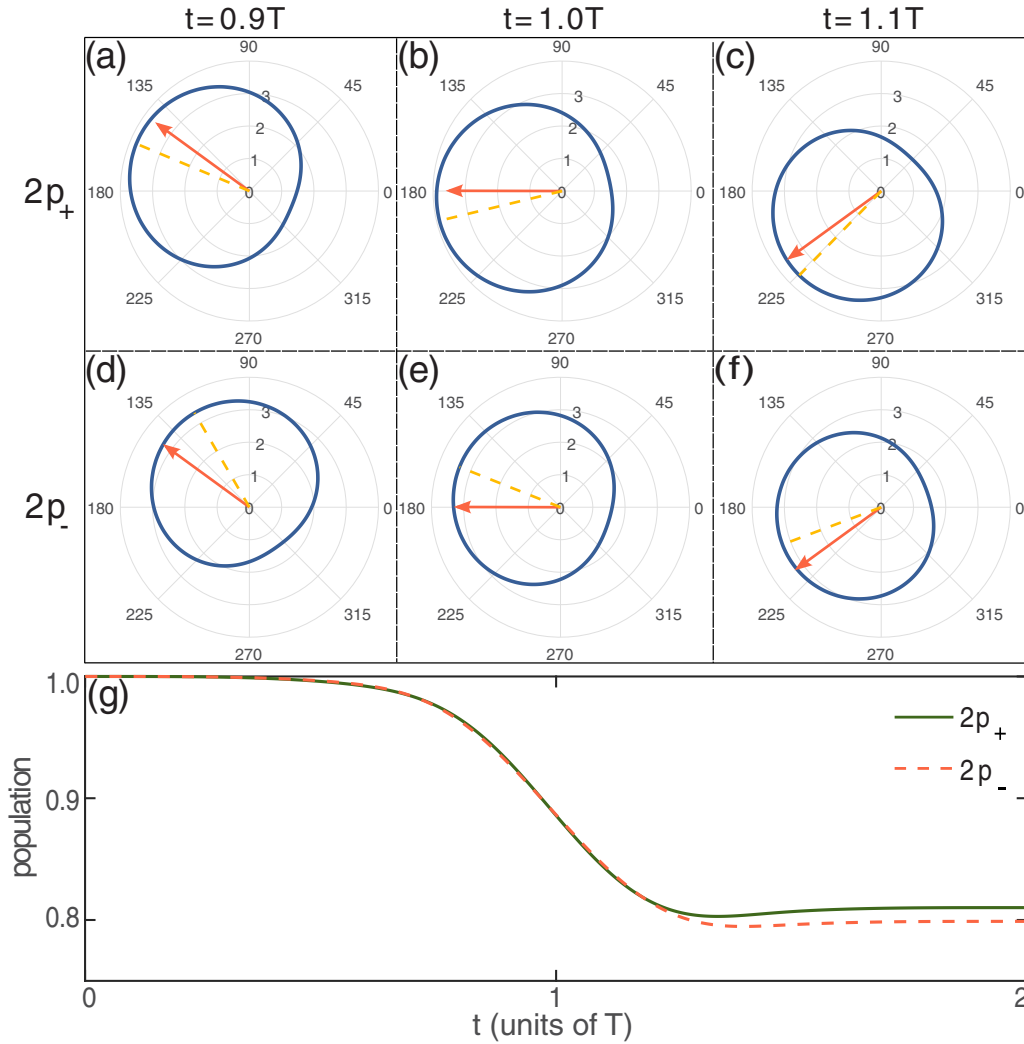
FIG. 6. (a)–(f) The electron probability densities (blue curves) at the circle located at $r(t) = I_p/|\mathbf{E}(t)|$ for three instants $0.9T$, $1.0T$, and $1.1T$. The densities are scaled by the factor 5×10^4 to better display the results. The arrows and dashed lines present the negative instantaneous field vector ($-\mathbf{E}$) and the maximum of the electron probability density, respectively. (g) The survival probabilities of the wave function with respect to the ionization time for the initial $2p_+$ (green solid line) and $2p_-$ (orange dashed line) orbitals.

phase spectroscopy to the attoclock technology. The results show that at the low laser intensity the ionization time delays are both close to zero for the $2p_\pm$ orbitals, though the most probable emission angles are different. The different offset angles are completely due to the long-range Coulomb interaction between the ion and the escaping electron, which is different for the two orbitals. As the laser intensity increases, the initial $2p_\pm$ orbitals are deformed by the short circularly polarized fundamental field. This deformation is different for the two orbitals. As a consequence, the ionization time delay is no longer the same for the $2p_\pm$ orbitals. With the increase of the laser intensity, the depletion of the ground state takes place,

which enhances the relative contribution of earlier ionization events to the PEMDs. As a result, the ionization time delay becomes negative for both orbitals.

[1] T. Zuo, A. D. Bandrauk, and P. B. Corkum, Laser-induced electron diffraction: A new tool for probing ultrafast molecular dynamics, Chem. Phys. Lett. **259**, 313 (1996).

[2] M. Lein, J. P. Marangos, and P. L. Knight, Electron diffraction in above-threshold ionization of molecules, Phys. Rev. A **66**, 051404(R) (2002).

[3] M. Meckel, D. Comtois, D. Zeidler, A. Staudte, D. Pavičić, H. C. Bandulet, H. Pépin, J. C. Kieffer, R. Dörner, D. M. Villeneuve, and P. B. Corkum, Laser-induced electron tunneling and diffraction, Science **320**, 1478 (2008).

[4] Y. Huismans, A. Rouzée, A. Gijsbertsen, J. H. Jungmann, A. S. Smolkowska, P. S. W. M. Logman, F. Lépine, C. Cauchy, S. Zamith, T. Marchenko, J. M. Bakker, G. Berden, B. Redlich, A. F. G. van der Meer, H. G. Muller, W. Vermin, K. J. Schafer, M. Spanner, M. Yu. Ivanov, O. Smirnova *et al.*, Time-resolved holography with photoelectrons, Science **331**, 61 (2011).

[5] Yueming Zhou, Oleg I. Tolstikhin, and Toru Morishita, Near-Forward Rescattering Photoelectron Holography in Strong-Field Ionization: Extraction of the Phase of the Scattering Amplitude, Phys. Rev. Lett. **116**, 173001 (2016).

[6] M. He, Y. Li, Y. Zhou, M. Li, W. Cao, and P. Lu, Direct Visualization of Valence Electron Motion Using Strong-Field Photoelectron Holography, Phys. Rev. Lett. **120**, 133204 (2018).

[7] J. Tan, Y. Zhou, M. He, Y. Chen, Q. Ke, J. Liang, X. Zhu, M. Li, and P. Lu, Determination of the Ionization Time Using Attosecond Photoelectron Interferometry, Phys. Rev. Lett. **121**, 253203 (2018).

[8] Y. Zhou, J. Tan, M. Li, and P. Lu, Probing the launching position of the electron wave packet in molecule strong-field tunneling ionization, Sci. China Phys. Mech. Astron. **64**, 273011 (2021).

[9] P. Eckle, M. Smolarski, P. Schlup, J. Biegert, A. Staudte, M. Schöffler, H. G. Muller, R. Dörner, and U. Keller, Attosecond angular streaking, Nat. Phys. **4**, 565 (2008).

[10] P. Eckle, A. N. Pfeiffer, C. Cirelli, A. Staudte, R. Dörner, H. G. Muller, M. Büttiker, and U. Keller, Attosecond ionization and tunneling delay time measurements in helium, Science **322**, 1525 (2008).

[11] C. Hofmann, A. Bray, W. Koch, H. Ni, and N. Shvetsov-Shilovski, Quantum battles in attoscience: Tunnelling, Eur. Phys. J. D **75**, 208 (2021).

[12] A. N. Pfeiffer, C. Cirelli, M. Smolarski, D. Dimitrovski, M. Abu-Samha, L. B. Madsen, and U. Keller, Attoclock reveals natural coordinates of the laser-induced tunnelling current flow in atoms, Nat. Phys. **8**, 76 (2012).

[13] L. Torlina, F. Morales, J. Kaushal, I. Ivanov, A. Kheifets, A. Zielinski, A. Scrinzi, H. Muller, S. Sukiasyan, M. Ivanov, and O. Smirnova, Interpreting attoclock measurements of tunnelling times, Nat. Phys. **11**, 503 (2015).

[14] H. Ni, U. Saalmann, and J.-M. Rost, Tunneling Ionization Time Resolved by Backpropagation, Phys. Rev. Lett. **117**, 023002 (2016).

[15] N. Eicke and M. Lein, Trajectory-free ionization times in strong-field ionization, Phys. Rev. A **97**, 031402(R) (2018).

[16] H. Ni, U. Saalmann, and J.-M. Rost, Tunneling exit characteristics from classical backpropagation of an ionized electron wave packet, Phys. Rev. A **97**, 013426 (2018).

[17] A. W. Bray, S. Eckart, and A. S. Kheifets, Keldysh-Rutherford Model for the Attoclock, Phys. Rev. Lett. **121**, 123201 (2018).

[18] M. Han, P. Ge, Y. Fang, X. Yu, Z. Guo, X. Ma, Y. Deng, Q. Gong, and Y. Liu, Unifying Tunneling Pictures of Strong-Field Ionization with an Improved Attoclock, Phys. Rev. Lett. **123**, 073201 (2019).

[19] C. Hofmann, A. S. Landsman, and U. Keller, Attoclock revisited on electron tunnelling time, J. Mod. Opt. **66**, 1052 (2019).

[20] N. Eicke and M. Lein, Attoclock with counter-rotating bicircular laser fields, Phys. Rev. A **99**, 031402(R) (2019).

[21] U. S. Sainadh, H. Xu, X. Wang, A. Atia-Tul-Noor, W. C. Wallace, N. Douguet, A. Bray, I. Ivanov, K. Bartschat, A. Kheifets, R. T. Sang, and I. V. Litvinyuk, Attosecond angular streaking and tunnelling time in atomic hydrogen, Nature (London) **568**, 75 (2019).

[22] N. Eicke, S. Brennecke, and M. Lein, Attosecond-Scale Streaking Methods for Strong-Field Ionization by Tailored Fields, Phys. Rev. Lett. **124**, 043202 (2020).

[23] V. V. Serov, A. W. Bray, and A. S. Kheifets, Numerical attoclock on atomic and molecular hydrogen, Phys. Rev. A **99**, 063428 (2019).

[24] V. V. Serov, J. Cesca, and A. S. Kheifets, Numerical and laboratory attoclock simulations on noble-gas atoms, Phys. Rev. A **103**, 023110 (2021).

[25] A. S. Landsman, M. Weger, J. Maurer, R. Boge, A. Ludwig, S. Heuser, C. Cirelli, L. Gallmann, and U. Keller, Ultrafast resolution of tunneling delay time, Optica **1**, 343 (2014).

[26] A. S. Landsman and U. Keller, Attosecond science and the tunnelling time problem, Phys. Rep. **547**, 1 (2015).

[27] A. Fortun, C. Cabrera-Gutiérrez, G. Condon, E. Michon, J. Billy, and D. Guéry-Odelin, Direct Tunneling Delay Time Measurement in an Optical Lattice, Phys. Rev. Lett. **117**, 010401 (2016).

[28] N. Teeny, E. Yakaboylu, H. Bauke, and C. H. Keitel, Ionization Time and Exit Momentum in Strong-Field Tunnel Ionization, Phys. Rev. Lett. **116**, 063003 (2016).

[29] Tomáš Zimmermann, S. Mishra, B. R. Doran, D. F. Gordon, and A. S. Landsman, Tunneling Time and Weak Measurement in Strong Field Ionization, Phys. Rev. Lett. **116**, 233603 (2016).

[30] N. Camus, E. Yakaboylu, L. Fechner, M. Klaiber, M. Laux, Y. Mi, K. Z. Hatsagortsyan, T. Pfeifer, Christoph H. Keitel, and Robert Moshammer, Experimental Evidence for Quantum Tunneling Time, Phys. Rev. Lett. **119**, 023201 (2017).

[31] R. Ramos, D. Spierings, I. Racicot, and A. M. Steinberg, Measurement of the time spent by a tunnelling atom within the barrier region, Nature (London) **583**, 529 (2020).

[32] I. Barth and O. Smirnova, Nonadiabatic tunneling in circularly polarized laser fields: Physical picture and calculations, Phys. Rev. A **84**, 063415 (2011).

[33] T. Herath, L. Yan, S. K. Lee, and W. Li, Strong-Field Ionization Rate Depends on the Sign of the Magnetic Quantum Number, Phys. Rev. Lett. **109**, 043004 (2012).

[34] I. Barth and O. Smirnova, Nonadiabatic tunneling in circularly polarized laser fields. II. Derivation of formulas, Phys. Rev. A **87**, 013433 (2013).

[35] I. Barth and M. Lein, Numerical verification of the theory of nonadiabatic tunnel ionization in strong circularly polarized laser fields, J. Phys. B: At., Mol. Opt. Phys. **47**, 204016 (2014).

[36] J. Kaushal, F. Morales, and O. Smirnova, Opportunities for detecting ring currents using an attoclock setup, Phys. Rev. A **92**, 063405 (2015).

[37] J.-P. Wang and F. He, Tunneling ionization of neon atoms carrying different orbital angular momenta in strong laser fields, Phys. Rev. A **95**, 043420 (2017).

[38] Q. Zhang, G. Basnayake, A. Winney, Y. F. Lin, D. Debrah, S. K. Lee, and W. Li, Orbital-resolved nonadiabatic tunneling ionization, Phys. Rev. A **96**, 023422 (2017).

[39] S. Eckart, M. Kunitski, M. Richter, A. Hartung, J. Rist, F. Trinter, K. Fehre, N. Schlott, K. Henrichs, L. Schmidt, T. Jahnke, M. Schöffler, K. Liu, I. Barth, J. Kaushal, F. Morales, M. Ivanov, O. Smirnova, and R. Dörner, Ultrafast preparation and detection of ring currents in single atoms, Nat. Phys. **14**, 701 (2018).

[40] D. Wu, F.-M. Guo, J.-G. Chen, J. Wang, and Y.-J. Yang, Ionization of an atom with different initial angular momenta in an intense circular polarized laser field, J. Phys. B: At., Mol. Opt. Phys. **53**, 235601 (2020).

[41] K. Liu, H. Ni, K. Renziehausen, J.-M. Rost, and I. Barth, Deformation of Atomic $p_{\pm}$ Orbitals in Strong Elliptically Polarized Laser Fields: Ionization Time Drifts and Spatial Photoelectron Separation, Phys. Rev. Lett. **121**, 203201 (2018).

[42] J. Yan, W. Xie, M. Li, K. Liu, S. Luo, C. Cao, K. Guo, W. Cao, P. Lan, Q. Zhang, Y. Zhou, and P. Lu, Photoelectron ionization time of aligned molecules clocked by attosecond angular streaking, Phys. Rev. A **102**, 013117 (2020).

[43] S. Skruszewicz, J. Tiggesbäumker, K.-H. Meiwes-Broer, M. Arbeiter, Th. Fennel, and D. Bauer, Two-Color Strong-Field Photoelectron Spectroscopy and the Phase of the Phase, Phys. Rev. Lett. **115**, 043001 (2015).

[44] V. A. Tulsky, M. A. Almajid, and D. Bauer, Two-color phase-of-the-phase spectroscopy with circularly polarized laser pulses, Phys. Rev. A **98**, 053433 (2018).

[45] J. Tan, Y. Li, Y. Zhou, M. He, Y. Chen, M. Li, and P. Lu, Identifying the contributions of multiple-returning recollision orbits in strong-field above-threshold ionization, Opt. Quantum Electron. **50**, 57 (2018).

[46] J. Tan, S. Xu, X. Han, Y. Zhou, M. Li, W. Cao, Q. Zhang, and P. Lu, Resolving and weighing the quantum orbits in strong-field tunneling ionization, Adv. Photonics **3**, 035001 (2021).

[47] M. D. Feit, J. A. Fleck, and A Steiger, Solution of the Schrödinger equation by a spectral method, J. Comput. Phys. **47**, 412 (1982).

[48] M. Protopapas, C. H. Keitel, and P. L. Knight, Atomic physics with super-high intensity lasers, Rep. Prog. Phys. **60**, 389 (1997).

[49] S. Chelkowski, C. Foisy, and A. D. Bandrauk, Electron-nuclear dynamics of multiphoton H_2^+ dissociative ionization in intense laser fields, Phys. Rev. A **57**, 1176 (1998).

[50] X. M. Tong, K. Hino, and N. Toshima, Phase-dependent atomic ionization in few-cycle intense laser fields, Phys. Rev. A **74**, 031405(R) (2006).

[51] X. M. Tong, S. Watahiki, K. Hino, and N. Toshima, Numerical Observation of the Rescattering Wave Packet in Laser-Atom Interactions, Phys. Rev. Lett. **99**, 093001 (2007).

[52] W. Yang, H. Zhang, C. Lin, J. Xu, Z. Sheng, X. Song, S. Hu, and J. Chen, Momentum mapping of continuum-electron wave-packet interference, Phys. Rev. A **94**, 043419 (2016).

[53] J. Tan, Y. Zhou, M. He, Q. Ke, J. Liang, Y. Li, M. Li, and P. Lu, Time-resolving tunneling ionization via strong-field photoelectron holography, Phys. Rev. A **99**, 033402 (2019).